ACI STRUCTURAL JOURNAL TECHNICAL PAPER

Title No. 119-S09

Flexural and Durability Performance of Seawater-Mixed Glass Fiber-Reinforced Polymer-Reinforced Concrete Slabs

by Carlos N. Morales, Guillermo Claure, and Antonio Nanni

Forty-eight simply supported glass fiber-reinforced polymer (GFRP) reinforced concrete (RC) slabs made with seawater-mixed concrete were tested to study potential performance degradation over different environmental conditions for 1, 6, 12, and 24 months. The environments consisted of typical field conditions of a subtropical region and immersion in seawater at 60°C (140°F) as an accelerated aging regimen. The GFRP-RC slab strips were 1828 mm (72 in.) long, 304 mm (12 in.) wide, and 152 mm (6 in.) deep and were reinforced with a 9.5 mm (0.375 in.) diameter GFRP bar. All the slabs were tested under three-point flexural loading and all exhibited bar rupture as the failure mode. The test results are reported in terms of the cracking load, ultimate moment capacity, and service-load deflections. Experimental results were compared to the analytical and ACI 440.1R-15 expected values. The type of concrete mixture design as well as the accelerated aging exposure seems to affect the ultimate capacity of GFRP-RC slabs. Analytical and ACI approaches reasonably predicted the experimental failure-moment capacity of most of the seawater-mixed GFRP-RC slabs, specifically for those exposed to field conditioning. The ACI 440.1R-15 equations were in good agreement with the experimentally measured deflections, where the largest deviations were observed for accelerated-aged specimens.

Keywords: cracking load; deflection; durability; fiber-reinforced polymer (FRP); flexural capacity; reinforced concrete.

INTRODUCTION

Reinforced concrete (RC) structures are usually reinforced with steel bars, yet it is widely recognized that structures exposed to harsh environments (for example, marine and offshore structures), as well as deicing salts, have a high risk of deterioration due to the corrosion of the steel reinforcement, the main reason of structural degradation.[1,2] It is estimated that in the United States alone, the annual direct cost of corrosion attributed to highway bridges (that is, reinforced concrete, prestressed concrete, and steel bridges) is $8.3 billion, plus an economic impact of indirect costs as high as 10 times the direct costs.[3] This explains the growing interest in structural systems that outperform current construction practices by providing superior long-term durability and low maintenance requirements.[4] In particular, nonconventional fiber-reinforced polymer (FRP) bars for concrete reinforcement have proven to be a suitable alternative to traditional corrosion-prone carbon steel reinforcing bar.[5] Among the most common types of fiber used to manufacture FRP reinforcing bars are glass, carbon, aramid, and basalt fibers.[6] Specifically, glass FRP (GFRP) with a vinyl ester resin is the most commonly used material system for manufacturing pultruded FRP bars,[7] as it is a cost-effective choice due to its high tensile strength, lightweight, and nonconductive and corrosion-resistant properties.[8] As expected, the mechanical behavior and long-term performance of GFRP bars when used as internal reinforcement in concrete differ from conventional steel reinforcement.

Conventional concrete is made with fresh water and river/quarry sand or desalted sea sand to limit potential detrimental chemical constituents such as chlorides that promote iron oxidation leading to corrosion of the steel reinforcement. By replacing steel with noncorrosive materials such as FRP bars, the alternative of using seawater and/or sea sand in the production of concrete, instead of conventional constituents, could be evaluated. The use of seawater-mixed concrete (seawater-mixed concrete and "seaconcrete" are used interchangeably in the text) has been of particular interest to researchers.[9-11] Xiao et al.[9] conducted a comprehensive literature review on the effects of using sea sand and/or seawater in the production of concrete. They reported that most studies show a higher compressive strength during the early stages and a similar long-term compressive strength compared to conventional concrete. However, Younis et al.[10] reported compressive strength of seaconcrete approximately 7 to 10% lower than concrete made with fresh water after 28 days, independently of curing conditions (fresh water or seawater). Furthermore, Khatibmasjedi et al.[11] reported a 14% higher compressive strength of seaconcrete than conventional concrete after 24 months of exposure to seawater at 60°C (140°F). In summary, it appears that additional research work may be needed to clarify the inconsistency in the strength behavior of seaconcrete compared to conventional concrete; however, it is expected that different mixture designs and curing regimens are likely to have different behaviors.

Typically, the physical and mechanical degradation of FRP bars has been evaluated by accelerated aging protocols, in which FRP bars are subjected to aggressive environmental conditioning for specific periods.[12-17] Discrepancies in the strength retention of FRP bars between accelerated aging and field exposure have also been reported.[12,18,19] It seems that direct exposure to a highly alkaline solution does not necessarily allow the prediction of the actual in-service real-life weathering. Researchers have also evaluated the degradation of FRP bars embedded in concrete, rather than exposing them directly to a solution. For this case, the literature reveals tensile strength retention of concrete-embedded

ACI Structural Journal, V. 119, No. 1, January 2022.

MS No. S-2020-386.R2, doi: 10.14359/51733006, received June 7, 2021, and reviewed under Institute publication policies.

GFRP bars between 59 and 93%.[20-25] However, only a few studies have been conducted specifically on the long-term durability performance of FRP bars embedded in concrete made with seawater instead of fresh water.[9] Test results showed that seaconcrete-embedded GFRP bars preserved between 50 and 85% of their initial tensile strength after exposure.[26,27] These fluctuations in strength retention can be attributed mainly to the bar diameter, type, and quality of the constituents (for example, fiber, sizing, and resin matrix), void content, temperature and time of exposure, and the surrounding medium (for example, concrete characteristics).

In contrast to the tensile strength reduction, either under accelerated conditioning or embedded in concrete, GFRP bars exhibited an equal or slightly higher residual tensile modulus of elasticity (E_f) over time. Nearly no change in E_f has been reported, regardless of the surrounding medium, environmental conditioning, or time of exposure.[14,15,17,18,20-22] This is a crucial point because for FRP-RC members, permissible deflection under service loads might control the design rather than the flexural strength requirements[8] (due to a relatively low E_f). Thus, for both compression-controlled and tension-controlled sections, the retention of E_f is of primary importance.

Numerous researchers have investigated the short-term flexural behavior of RC slabs reinforced with FRP bars.[28-39] Most of the published research on this topic has been performed using conventional concrete, and virtually none with seaconcrete. Gao et al.[40] conducted a study to evaluate the flexural and blast response of one-way slabs reinforced with 6 mm (0.24 in.) diameter basalt FRP (BFRP) bars. In the study, slabs were cast with two different concrete mixture designs: sea-sand seaconcrete and conventional freshwater concrete. In particular, the three-point bending flexural test results showed a 13% difference between BFRP-RC slabs made with sea-sand seaconcrete and conventional concrete subjected to the same conditions.

In addition to FRP-seaconcrete slabs, the durability and flexural performance of beams made with seawater and reinforced with FRP bars have been further studied. Dong et al.[41] performed accelerated aging tests (artificial seawater at 50°C [122°F]) on seawater sea-sand concrete beams reinforced with 13 mm (0.51 in.) diameter BFRP bars. They reported changes in the failure mode (from concrete crushing to shear failure) of BFRP-RC beams after 9 months of accelerated conditioning, mostly attributed to the degradation of the FRP-to-concrete bond. More recently, Younis et al.[42] conducted a research study to investigate the short-term flexural performance of GFRP-RC beams made with seawater recycled-aggregate concrete. The GFRP-RC beams were reinforced with 12 mm (0.47 in.) diameter GFRP bars and tested under four-point loading after 2 months of concrete casting. They concluded that using seawater and recycled coarse aggregate in concrete has insignificant effects on the flexural capacity compared to different concrete mixtures with comparable compressive strength.

This study aims to evaluate the flexural and durability performance of one-way GFRP-RC slab strips made with seaconcrete. Different seaconcrete mixture designs and environmental conditions were evaluated over several periods. The environmental exposures consisted of typical field conditions of a subtropical region and seawater at 60°C (140°F) as accelerated aging. The experimental results of the simply supported GFRP-RC slabs were assessed and compared based on the ultimate capacity, cracking load, and midspan deflection. In addition, a two-way analysis of variance (ANOVA) was performed to determine the interaction between the time of exposure and environmental conditioning. The statistical differences were reported in terms of the ratio between-group variation to within-group variation (F-ratio) and the probability that a result has occurred by change (p-value). A level of significance $p < 0.05$ (that is, 5%) was considered statistically significant, as typically employed in statistics.[43]

RESEARCH SIGNIFICANCE

It has been widely recognized that FRP reinforcing bars have the potential to contribute to solving the issue of corrosion in RC structures due to their noncorrosive properties. By not having to deal with corrosion degradation, seawater-mixed concrete can be considered for use together with noncorrosive reinforcement. Considerable research has been conducted on the behavior of one-way simply supported GFRP-RC slabs; however, nearly all was limited to the short-term performance and the use of conventional concrete. This paper examines the flexural and durability performance of simply supported GFRP-RC slab strips made with seawater-mixed concrete exposed to the field and accelerated aging regimens over short and long periods.

EXPERIMENTAL INVESTIGATION

Materials

Seaconcrete—In this study, two different seaconcrete mixture designs and environmental conditions were evaluated over several periods. The selected designs were based on the Infravation-funded international collaborative research project named SEACON, in which an extensive and detailed evaluation of the properties of the fresh and hardened state of concrete made with seawater was conducted (further details can be found in other studies[11,26,44,45]). Both seaconcrete mixture designs, referred to in this study as Mixture Type-F and Mixture Type-S, had a target 28-day compressive strength of 38 MPa (5500 psi). Mixture Type-F had a fly ash cement replacement level of 20%ωt, while Mixture Type-S had a slag cement (SC) replacement level of 50%ωt. The use of fly ash and slag is recognized to improve the performance of hardened seawater-mixed concrete.[11,46,47]

The seawater used to mix the concrete, as well as for the accelerated-aging conditioning, was obtained directly from Biscayne Bay, FL, with a pH value of 8.23. Additional details on the chemical composition of the seawater used in this study are provided in parallel studies.[26,48] Table 1 provides details of the proportions for each mixture. Concrete cylinders with a diameter of 100 mm (4 in.) and a height of 200 mm (8 in.) were cast along with each group of slabs to evaluate compressive strength development over time according to ASTM C39.[49] For each particular seaconcrete mixture design, all concrete elements were cast from a single batch using a concrete truck.

GFRP bar—The pultruded 9.5 mm (0.375 in.) nominal diameter GFRP bars used in this study were fabricated from continuous electrical corrosion resistance (ECR)-glass with a fiber content of 85% (by weight) determined according to ASTM D2584[50] impregnated in a vinyl ester resin matrix. The surface enhancement consisted of a double-helical fiber-wrapped surface creating a small 45-degree braided surface pattern undulation. The physical and mechanical properties of pristine GFRP bars were determined according to the established test methods indicated in ASTM D7957.[51] The property, test method, experimental value, and coefficient of variation (CV %) for each test are given in Table 2. The measured cross-sectional area closely approached the nominal value specified in ASTM D7957[51] for an M10 (No. 3) GFRP bar (percentage error approximately 1%). The mechanical properties (that is, ultimate and guaranteed tensile strength, modulus of elasticity, and ultimate strain) of the GFRP bars were tested per ASTM D7205[52] and calculated using the measured cross-sectional area.[53]

Table 1—Seaconcrete mixture proportions (adapted from SEACON[44])

Material	Mixture Type-F	Mixture Type-S
	kg/m^3 (gal./yd^3)	
Portland cement	332 (560)	208 (350)
Fly ash	83 (140)	—
Slag	—	208 (350)
Seawater	168 (283)	158 (267)
Coarse aggregate	1038 (1750)	997 (1680)
Fine aggregate	612 (1032)	691 (1165)
—	mL/m^3 (gal./yd^3)	
Set-retarding admixture	830 (0.2)	2179 (0.4)
Air-entraining admixture	310 (0.1)	20 (0.004)
Water-reducing admixture	—	817 (0.2)
—	*w/cm*	
—	0.40	0.38

Note: *w/cm* is water-cementitious materials ratio.

Specimens

In this study, 48 test specimens representing a strip of one-way simply supported GFRP-RC slab made with seaconcrete mixture designs Type-F and Type-S were investigated. All the slabs had a span of 1524 mm (60 in.) and were constructed with a cross-sectional area of 152 by 304 mm (6 x 12 in.) and a length of 1828 mm (72 in.), as shown in Fig. 1. All the slabs were reinforced with a single 9.5 mm diameter (0.375 in.) GFRP bar, selected from the same batch. The clear concrete cover was 19 mm (0.75 in.). The use of a single M10 (No. 3) GFRP bar was to provide a tension-controlled failure. This choice guarantees the limit state of GFRP rupture as the failure parameter necessary for evaluating reinforcement degradation.

After the 28-day moist curing, half of the concrete specimens (slabs and cylinders) were exposed to a typical subtropical field environment, while the other half were completely submerged in temperature-controlled seawater inside several polyurethane tanks at a constant temperature of 60°C (140°F). Figure 2 illustrates the experimental setup for the accelerated conditioning. The chosen temperature of 60°C (140°F) for the accelerated-aging protocol is well below the glass transition temperature (T_g) of the GFRP bars used in this study, which is approximately 112°C (234°F). Although this is not an exposure that structures experience in common applications, lower tensile strength retention has been reported for GFRP bars embedded in continuously submerged concrete than for those subjected to

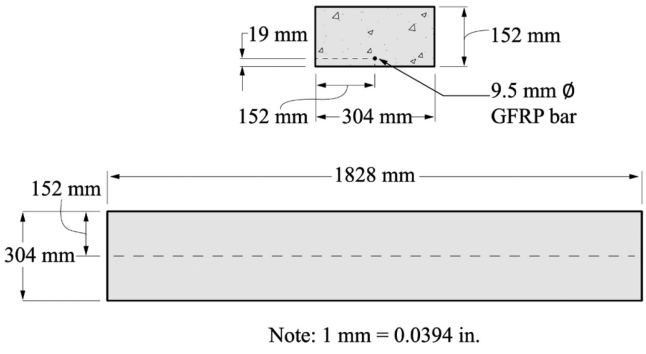

Fig. 1—GFRP-RC slab geometry: cross section (top); and top view (bottom).

Table 2—Physical and mechanical characterization of GFRP bars

—	Property	Unit	Test method	Value	CV %
Physical properties	Effective diameter	mm (in.)	ASTM D7205	9.56 (0.376)	0.24
	Cross-sectional area	mm^2 (in.^{2})	ASTM D792	71.81 (0.111)	0.49
	Density	kg/m^3 (lb/ft^3)	ASTM D792	2179.6 (136.1)	0.22
	Fiber content	% by weight	ASTM D2584	85.06	0.24
		% by volume	SEM*	71.09	6.2
Mechanical properties	Tensile strength	MPa (ksi)	ASTM D7205	822.23 (119.25)	4.7
	Guaranteed tensile strength†	MPa (ksi)	ASTM D7205	705.96 (102.4)	—
	Tensile modulus	GPa (ksi)	ASTM D7205	55.04 (7983)	2.0
	Ultimate tensile strain	%	ASTM D7205	1.49	5.2

*By digital image processing of SEM images.[53]

†Guaranteed tensile strength, (f_{fu}^*), equal to mean tensile strength of test specimens minus three times standard deviation.

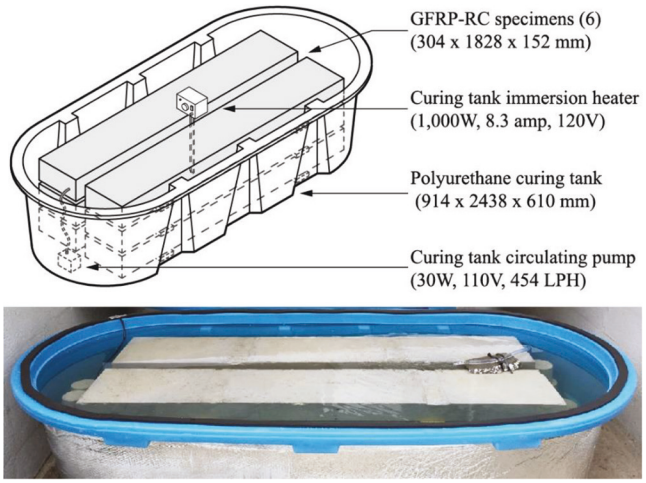

Fig. 2—Accelerated-aging setup (seawater at 60°C [140°F]).

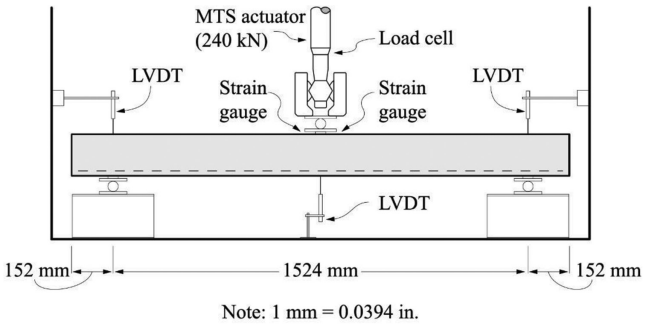

Fig. 3—Experimental setup of simply supported GFRP-RC slab.

wetting-and-drying cycles (seawater at 50°C).[21] At the same time, the samples exposed to the field environment were subjected to a climate with an average ambient temperature of 25.7°C (78.3°F) and average relative humidity (RH) of 71.2%.

The corresponding nomenclature for the GFRP-RC slabs was based on the type of mixture design, exposure conditioning, and time of exposure. The first letter in the nomenclature denotes the type of mixture design—that is, letter F for the mixture design made using fly ash and the letter S for the one made with slag. The second segment denotes the exposure conditioning, "FC25" for field conditioning at 25°C and "SW60" for specimens conditioned in seawater at 60°C (140°F). Lastly, the third portion represents the exposure time in months: 1, 6, 12, and 24 months. For example, "F-FC25-24" corresponds to concrete elements cast with mixture design Type-F exposed to field conditioning at a temperature of 25°C for 24 months.

Test setup

The flexural behavior of the GFRP-RC slabs was determined by placing the slabs between two supports with a clear span of 1524 mm (60 in.) and loaded at the midspan using a 240 kN (55 kip) hydraulic universal test frame, as shown in Fig. 3. The applied load was measured using the internal force transducer. Linear variable differential transducers (LVDTs) were used to measure the midspan deflection and any settlement in both supports. In addition, the compressive strain was also measured and recorded using two electrical resistance strain gauges attached to the outer face of the concrete, located at half-width of the top surface at equal distances from each side of the point load. All test data were recorded simultaneously using a multiple portable data acquisition (DAQ) system.

All the GFRP-RC slabs were tested under two control conditions throughout the three-point bending flexural test. Load control, at a rate of 0.222 kN/s (50 lb/s), was used during the initial phase of the test in four loading-unloading sequences equivalent to 50, 67, 83, and 100% of the test load magnitude, which is defined as 85% of the ultimate design load capacity for tension-controlled specimens, as per ACI 437-12.[54] After reaching each load step increment, the load was held for 2 minutes and then the specimen was unloaded to 10% of the ultimate design load capacity. Each of the sequences was performed twice in succession to show the hysteresis of the loading-unloading cycles that may contribute to the element's energy absorption and dissipation capacity. After the first loading protocol was completed, the load was applied to the slabs until failure under a displacement-controlled monotonic loading rate of 0.0318 mm/s (0.00125 in./s) to allow for controlled crack propagation. This study focused on the latter protocol because the RC elements were mostly uncracked (linear elastic behavior) during the first phase. Three repetitions of the flexural test per mixture design and exposure conditioning were performed after 1, 6, 12, and 24 months of exposure.

Flexural behavior—analysis and procedure

Design and predicted capacity—The flexural strength capacity of an FRP-RC member can be determined based on the strength limit states in which the failure is controlled by either concrete crushing or FRP bar rupture.[8] In a given section, when the FRP reinforcement ratio, ρ_f (= A_f/bd, where A_f is the total area of the FRP bars; b is the width of the rectangular cross section; and d is the effective depth of the slab section), is less than the balanced ratio, ρ_{fb}, the failure is controlled by FRP bar rupture (tension-controlled section); otherwise, it is governed by the concrete crushing limit state. The balanced failure strain condition occurs when the concrete strain reaches its ultimate capacity, at the same time the outermost FRP bar layer reaches its strain capacity. According to ACI Committee 440, the balanced FRP reinforcement ratio is computed as follows

$$\rho_{fb} = 0.85\beta_1 \frac{f_c'}{f_{fu}} \frac{E_f \varepsilon_{cu}}{E_f \varepsilon_{cu} + f_{fu}} \quad (1)$$

where f_c' is the specified compressive strength of concrete; f_{fu} (= $C_E f_{fu}^*$, where C_E is the environmental reduction factor) is the ultimate tensile strength of FRP bars (as FRP does not yield); ε_{cu} is the ultimate strain of concrete (taken as 3000 με); and β_1 is the strength reduction factor taken as 0.85 for concrete compressive strength equal to or less than 28 MPa (4000 psi). For strength exceeding 28 MPa (4000 psi), the factor β_1 is reduced continuously at a rate of 0.05 for every

7 MPa (1000 psi) of strength above 28 MPa (4000 psi) with a threshold not less than 0.65. The E_f can be taken as the mean elastic modulus value reported by the manufacturer.

Because in this study the GFRP-RC slabs were "under-reinforced," this section solely reviews when failure is determined by rupture of the FRP reinforcement. In a tension-controlled section, given that the f_{fu} is reached first (ε_{cu} is less than 3000 με), the depth of the neutral axis c is unknown. In this case, the ACI equivalent rectangular stress block parameters are not applicable. Therefore, it is required to compute the neutral axis location based on the equilibrium and strain compatibility, as well as the nonlinear stress distribution of the concrete. The corresponding stress distribution in the concrete can be approximated with an equivalent rectangular stress block using two strain- and stress-dependent parameters, β and α.[55] Several stress-strain models have been proposed to interpret the behavior of concrete,[56] with the one proposed by Todeschini et al.[57] being one of the most used. The equivalent stress block parameters for Todeschini's model can be calculated as follows[55,58,59]

$$\beta = 2 - \frac{4\left[\left(\varepsilon_c / \varepsilon_c'\right) - \tan^{-1}\left(\varepsilon_c / \varepsilon_c'\right)\right]}{\left(\varepsilon_c / \varepsilon_c'\right)\ln\left[1 + \left(\varepsilon_c / \varepsilon_c'\right)^2\right]} \tag{2}$$

$$\alpha = \frac{0.90\ln\left[1 + \left(\varepsilon_c / \varepsilon_c'\right)^2\right]}{\beta\left(\varepsilon_c / \varepsilon_c'\right)} \tag{3}$$

where ε_c is the compressive strain in concrete; and ε_c' represents the concrete strain corresponding to f_c', calculated as $\varepsilon_c' = 1.71(f_c'/E_c)$. The modulus of elasticity of concrete (E_c) can be calculated by the simplified equation suggested by ACI 318-19[60] as $E_c = 4700\sqrt{f_c'}$ MPa for normalweight concrete.

Based on the stress distribution of a tension-controlled section and applying the compatibility internal force equilibrium, where the resultant of the compressive stress in the concrete equals the tensile force in the reinforcement, the following expression can be made

$$A_f f_{fu} = \beta\alpha f_c' \, bc \tag{4}$$

where c is the distance from the extreme compression fiber to the neutral axis.

In this study, the analytical method used to determine the nominal moment capacity was based on the iterative approach. First, a depth of a neutral axis, c, ($c < c_b$) was assumed so that the parameters ε_c, β, and α could be calculated. Then, using the equilibrium expression (Eq. (4)) a "new" c was computed. This was iterated until convergence between the assumed neutral axis and the computed one was achieved. Lastly, the analytical nominal moment capacity ($M_{n(an)}$) was determined using the final values obtained for β and c as follows

$$M_{n(an)} = A_f f_{fu}\left(d - \frac{\beta c}{2}\right) \tag{5}$$

The nominal capacities calculated using this method were defined as the analytical solution ($M_{n(an)}$). The strain-compatibility approach is suggested to be applied in cases where multiple layers of reinforcement and combinations of different types of FRP are used.[8]

At the same time, for a tension-controlled section, ACI 440.1R-15[8] provides a simplified calculation of the nominal flexural strength. This approach allows the use of the equivalent rectangular stress block (irrespectively of the strain reached by the concrete) and the use of the neutral axis depth for balance failure determined as

$$c_b = \left(\frac{\varepsilon_{cu}}{\varepsilon_{cu} + \varepsilon_{fu}}\right)d \tag{6}$$

Under these assumptions, the approximate nominal capacity provided in ACI 440.1R-15[8] can be calculated as follows

$$M_{n(ACI)} = A_f f_{fu}\left(d - \frac{\beta_1 c_b}{2}\right) \tag{7}$$

Because in a tensile-controlled section $c < c_b$, the bending moment capacity calculated using Eq. (7) is considered a conservative lower-bound estimate. The predicted nominal capacities calculated using Eq. (7) were labeled as the ACI solution ($M_{n(ACI)}$).

Additionally, ACI Committee 440 recommends estimating the cracking moment (M_{cr}) capacity as follows

$$M_{cr} = \frac{0.62\lambda\sqrt{f_c'}\, I_g}{y_t} \tag{8}$$

where λ is the modification factor for lightweight concrete; I_g (= $bh^3/12$ where h is the height of the cross section) is the gross moment of inertia; and y_t is the distance from the centroidal axis of the gross section to the top face. The f_c' used in Eq. (8) were those obtained in the compressive strength test of concrete cylinders, which were tested at the same time as the flexural tests. Subsequently, the predicted cracking loads ($P_{cr\ pre}$) were back-calculated from the cracking moment capacity equation.

Prediction of midspan deflection—The instantaneous predicted deflections were calculated according to ACI 440.1R-15[8] using standard structural analysis techniques for a simply supported slab under a concentrated load at the midspan ($\Delta = PL^3/48E_cI$, where P is the applied load; L is the total span length; and I is the moment of inertia). For an uncracked section, the moment of inertia is equal to the gross moment of inertial (I_g). Once the applied moment surpasses the cracking moment, the overall flexural stiffness decreases, leading to the following effective moment of inertia as per ACI 440.1R-15[8]

$$I_e = \frac{I_{cr}}{1 - \gamma\left(\frac{M_{cr}}{M_a}\right)^2\left[1 - \frac{I_{cr}}{I_g}\right]} \tag{9}$$

where M_a is the applied moment; γ is a parameter used to account for the variation in stiffness along the length of the slab suggested by Bischoff and Gross,[61] as $\gamma = 3 - 2(M_{cr}/M_a)$ for a simply supported span with a concentrated load at midspan; and $I_{cr} = (bd^3/3)k^3 + n_f A_f d^2(1-k)^2$ is the transformed moment of inertial of a cracked section where $k = \sqrt{2\rho_f n_f + (\rho_f n_f)^2} - \rho_f n_f$ is the ratio of the neutral axis to the reinforcement depth and $n_f = E_f/E_c$. The effective moment of inertia (I_e) and the conventional structural analysis equations were used to calculate the predicted instantaneous post-crack deflections.

EXPERIMENTAL RESULTS AND DISCUSSION

Concrete compressive strength

A minimum of three concrete cylinders were tested for each exposure conditioning and period to assess the strength development over time. After 28 days of moist curing (moist room at 100% RH and temperature of 23 ± 1°C [73.4 ± 2°F]), the average compressive strength of seaconcrete Type-F and Type-S were 41.6 MPa (6040 psi) and 37.3 MPa (5414 psi), respectively. Figure 4 shows the compressive strength development of the concrete cylinders that were exposed to the same time and environmental conditioning as the GFRP-RC slabs, in addition to the cylinders that were continuously cured in the moist room (MR23).

In the case of concrete Type-S, a decrease of 13% was observed for the 6-month exposure period (with respect to the previous one); then, almost no change between the 12-month period and the last period. This concrete compressive strength behavior is not in line with those reported in the literature for SC-blended concrete made with seawater[47,62,63] (which increases strength gradually). However, because the concrete constituents were dosed at a concrete batching plant and delivered using a concrete truck, caution should be taken when interpreting the results due to the greater potential for variability than in a controlled laboratory environment. Nonetheless, these outcomes could be considered practical, as they would allow for a more realistic and representative large-scale concrete production scenario taking into account that, even with the unexpected behavior, the compressive strengths were above the target 28-day compressive strength.

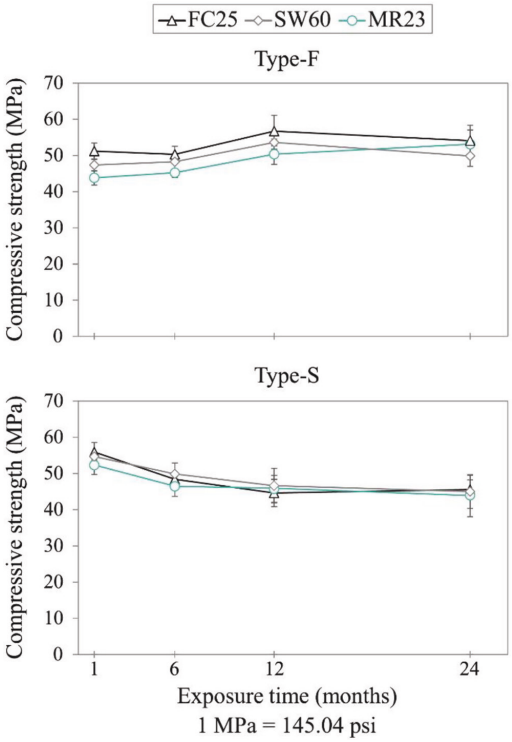

Fig. 4—Seaconcrete compressive strength over time of exposure. Error bars represent standard deviation.

After 24 months of exposure, the concrete samples submerged in seawater at 60°C (140°F) (SW60) exhibited compressive strength comparable to that of samples exposed to the field environment (FC25) with an average difference of 8.2% and 1.3% for concrete Type-F and Type-S, respectively. The two-way ANOVA showed no statistically significant interaction between the effects of environmental conditioning and exposure time on the compressive strength: $F = 0.516$ and $p = 0.725$ for specimens made with concrete Type-F, and $F = 0.322$ and $p = 0.860$ for specimens made with concrete Type-S. These results are in agreement with the literature.[11] Conversely, the environmental conditioning exposure for concrete cylinders made with Mixture Type-F seems to have an effect ($p = 0.021$), but not for Mixture Type-S ($p = 0.758$). When comparing the samples cured in the moist room (MR23), the difference in compressive strength of the concrete cylinders made with concrete Type-F that were exposed to FC25 and SW60 was 1.8% and 6.4%, respectively. Similarly, comparable results were also measured for the cylinders made with concrete Type-S, with a difference of 3.8% and 2.4% for exposures FC25 and SW60, respectively. Further details on the mechanical and durability properties of concrete can be found in Morales et al.[45]

Three-point bending flexural test and general behavior

Concrete cracking load—In general, the crack pattern for all the GFRP-RC slab groups was similar regardless of concrete mixture design, exposure time, and environmental conditioning. Typical flexural crack patterns after 24 months of exposure are shown in Fig. 5. The cracking pattern of the concrete slabs initiated on the tension face at the midspan and spread upwards to the point of load application. After the first crack, and as the load increased, a few other cracks appeared scattered near the center. As the load progressively increased, the width of the cracks increased and propagated from adjacent regions toward the upper loading point.

For both mixture designs, the maximum flexural load was plotted against the average measured compressive strain (ε_{cu}) obtained from the two concrete strain gauges and is shown in Fig. 6. These values represent the maximum strain values obtained in the outermost compression fiber of the concrete when the maximum load was applied just before failing (bar rupture). As expected, higher loads lead to higher compression strain. The measured compressive strain values, considering both mixture designs, ranged between 200 and 1000 με, which are well under the assumed maximum concrete compressive strain of 3000 $\mu\varepsilon_{cu}$ suggested by ACI 318-19.[60] The relationships are practically linear because the materials

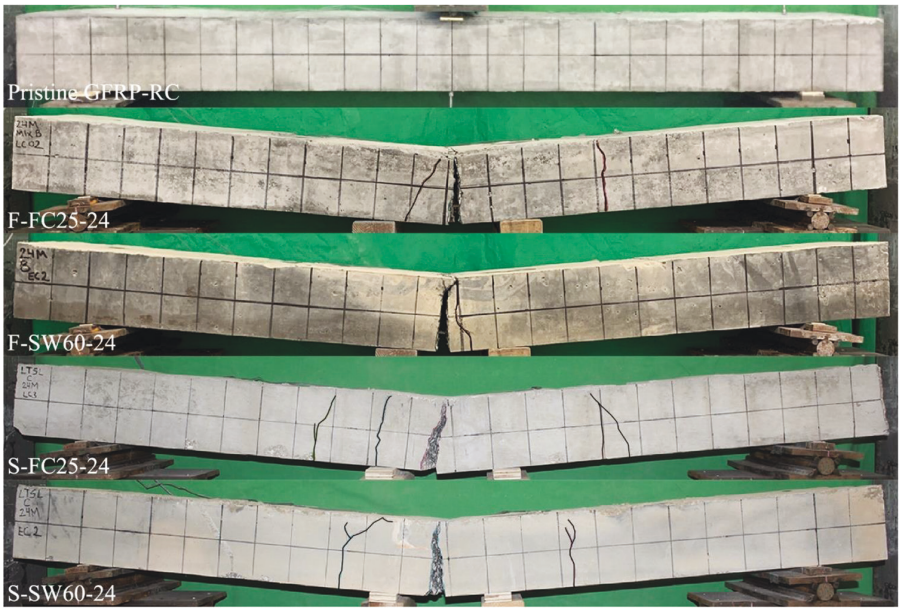

Fig. 5—Typical flexural crack pattern of tested GFRP-RC slabs after 24 months of exposure.

remain linear at the time of failure. This confirms the occurrence of tensile rupture of the GFRP bar prior to concrete crushing.

Ultimate load capacity—All the tested slabs exhibited a tension-controlled failure (Fig. 7). Failure of the GFRP-RC slabs was characterized by progressive sounds of fiber breakage, just before sudden GFRP bar rupture accompanied by a loud sound. The average failure loads of the GFRP-RC slabs made with seaconcrete Type-F are shown in Fig. 8. Independently of the exposure time, the slabs subjected to accelerated aging (SW60) showed an average ultimate capacity lower than those exposed to field conditioning (FC25). After 24 months of exposure, the average failure load of the F-FC25 group was 13.8% of the F-SW60 group. The two-way analysis revealed that the interaction effect between the exposure time and environmental conditioning was not statistically significant: $F = 0.40$ and $p = 0.752$. However, an analysis of the main effect of environmental conditioning indicated that there was a statistically significant effect: $F = 15.27$ and $p < 0.002$. Therefore, that for GFRP-RC slabs made with concrete mixture design Type-F, the accelerated exposure protocol (seawater at 60°C [140°F]) had a statistically significant effect on the flexural performance compared to field conditioning.

Figure 9 shows the average failure loads of the GFRP-RC slabs made with the seaconcrete Mixture Type-S. Similar to the specimens made with Mixture Type-F, it is evident that the environmental conditioning affected the ultimate flexural capacity. The difference in ultimate capacity between the S-FC25 and S-SW60 specimens after 24 months of exposure was 17.5%. The two-way analysis revealed no statistically significant differences between the interaction of the exposure time and environmental conditioning: $F = 1.0$ and $p = 0.417$. Yet, there was a highly statistically significant main effect of environmental conditioning: $F = 28.10$ and $p < 0.0001$.

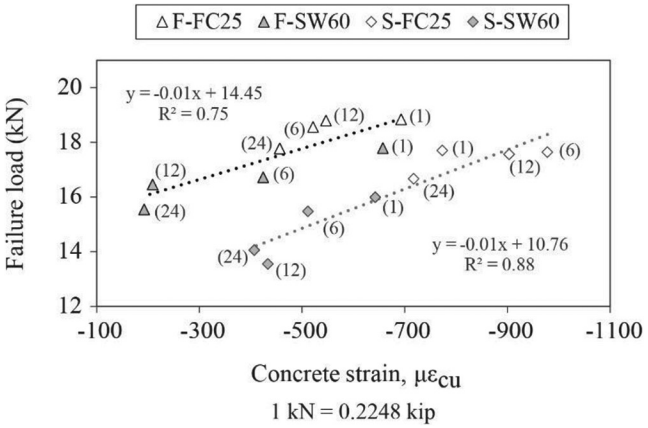

Fig. 6—GFRP-RC failure load versus concrete strain on compression face. Times of exposure are shown in parentheses.

Comparison of predicted and experimental capacity

The analytical and ACI-predicted nominal moment capacities were calculated according to Eq. (5) and (7), respectively. These flexural capacities were computed using measured mechanical properties such as the experimental f_{fu}, E_f, and A_f. Additionally, all reduction factors, including the environmental (C_E) and strength reduction factor (ϕ) were assigned to be equal to 1 for comparison purposes.

The design moment capacity ($M_{des} = \phi M_{n(ACI)}$) was calculated using Eq. (6) and (7), along with the following parameters: the target f_c' (38 MPa [5500 psi]); the environmental reduction factor for GFRP bars embedded in the concrete exposed to earth and weather ($C_E = 0.7$); the strength reduction factor for tension-controlled sections ($\phi = 0.55$); and the minimum guaranteed tensile strength (f_{fu} = 579 MPa [84 ksi]) and the nominal area ($A_n = 71$ mm^2 [0.11 in.^{2}]) for a 9.5 mm (0.375 in.) diameter GFRP bar. The calculated M_{des} resulted in a flexural strength of 2.69 kN·m (1.99 ft·kip). It should be noted that because the rupture of the GFRP bar

Fig. 7—Typical GFRP bar tensile rupture failure at midspan.

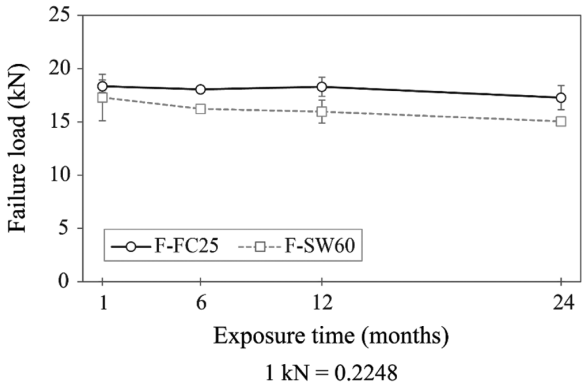

Fig. 8—Average load capacity of GFRP-RC slabs made with concrete Mixture Type-F. Error bars represent standard deviation.

Table 3—Effect of f_c' on design moment capacity

f_c', MPa (psi)	M_{des}, kN·m (ft·kip)
37.92 (5500)	2.69 (1.99)
41.37 (6000)	2.70 (1.99)
44.82 (6500)	2.71 (2.0)
48.26 (7000)	2.72 (2.0)

controlled the slabs' failure, variations in f_c' on the design moment capacity (M_{des}) were minimal, as shown in Table 3.

Table 4 presents the average flexural test results (set of three) and the analytical and ACI-predicted nominal moment capacities, as well as the ratio of the experimental to the computed values of all the GFRP-RC slabs. The mean ratio between the experimental and the analytical predicted failure values ($M_{exp}/M_{n(an)}$) for the GFRP-RC slabs made with concrete Type-F were 0.97 and 0.87 for F-FC25 and F-SW60 conditioning, respectively, while for slabs made with concrete Type-S, these values were 0.91 and 0.78 for S-FC25 and S-SW60, respectively.

For the GFRP-RC slabs made with concrete Type-F, the ratio of the experimental to predicted ACI nominal capacity ($M_{exp}/M_{n(ACI)}$) were 1.0 and 0.90 for F-FC25 and F-SW60, respectively, whereas, for slabs made with concrete Type-S, the ratios were 0.94 to 0.80 for S-FC25 and S-SW60, respectively. Based on these results, the GFRP-RC slabs made with concrete Type-F were in better agreement with the predicted moment capacity than the slabs made with concrete Type-S. Comparatively, the ACI-predicted moment capacity was on average 3% less than the analytically calculated values, as expected due to the simplified lower-bound approach.

In the same way, the experimental moment capacity (M_{exp}) was compared to the ACI 440.1R-15[8] design capacity (M_{des}), as shown in Table 4. The ratio between the experimental and the design values, including both mixture designs, ranged between 2.13 and 2.65. It is noted that the knock-down factors (that is, C_E, ϕ, and f_{fu}^*) accounting for different uncertainties make the design conservative even when the seaconcrete samples are subject to accelerated conditioning.

The crack load values obtained from the flexural tests ($P_{cr\,exp}$), as well as those calculated ($P_{cr\,pre}$), and the comparison between the two ($P_{cr\,exp}/P_{cr\,pre}$) are shown in Table 5. On average, the slabs made with concrete Type-F cracked at 8% and 3% below the predicted ACI Committee 440 cracking loads for F-FC25 and F-SW60 conditioning, respectively. For the slabs made with concrete Type-S, the first crack occurred at 37% and 22% below the predicted capacities for S-FC25 and S-SW60 exposures, respectively. Although the cracking loads were overestimated, it was evident that $P_{cr\,pre}$ values were much closer to the experimental values for the slabs made with concrete Type-F than to those made with concrete Type-S.

Load-deflection behavior

Figure 10 shows the experimental load-deflection response at the midspan obtained from the three-point bending flexural tests for the seaconcrete GFRP-RC slabs made with concrete Type-F and Type-S. Because the slabs within each group exhibited similar behavior, a representative load-deflection curve per time of exposure is shown. Additionally, for the legibility of the graphs, the unload-reload steps were omitted.

Prior to ultimate failure, the load-deflection response can be divided into two parts: pre- and post-cracking performance. Throughout the first part, the slabs exhibited a linear load-deflection behavior up to the first crack load, where the applied load exceeded the cracking moment capacity. The second part was characterized by a prominent reduction in bending stiffness and, as the load continuously increased, further cracks developed, leading to sudden reductions in the applied load and a less steep load-deflection behavior. Finally, the slabs failed abruptly without warning, as expected, because FRP bars lack plastic behavior. Overall, this load-deflection response is expected because FRP-RC elements have a relatively small post-cracking stiffness due

to a relatively low modulus of elasticity compared to steel-reinforced concrete elements with the same reinforced ratio.[8]

For comparison purposes, the ACI-predicted post-crack load-deflection curve (based on the design parameters) was also plotted in Fig. 10. Because for most slabs, the experimental crack onset load differs greatly from the predicted values, the starting point of the predicted post-crack response was made to coincide with the average experimental load where the load-deflection curve started to reascend after the first abrupt load drop (due to the first crack).

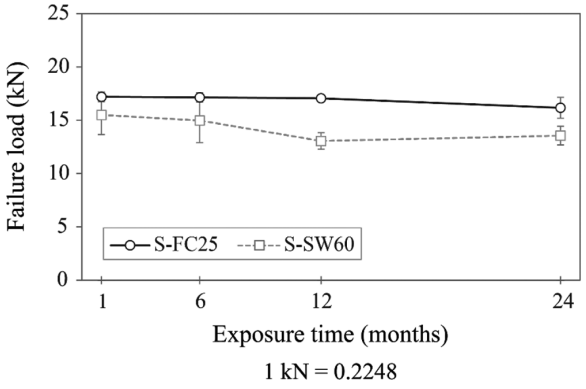

Fig. 9—Average load capacity of GFRP-RC slabs made with concrete Mixture Type-S. Error bars represent standard deviation.

Additionally, the nominal (including/excluding C_E and ϕ), design, and service load thresholds were displayed in Fig. 10 as horizontal dashed lines. The service moment capacity was calculated by considering the ultimate load to 1.2 times the dead load (D_L) plus 1.6 times the live load (L_L) and assuming $L_L = 2D_L$. This resulted in a service level moment of approximately 70% of M_{des} and 38.5% of $M_{n(ACI)}$. Then, the service load (P_{serv}) and the ultimate design flexural capacity (P_{des}), due to a point load at the midspan, were back-calculated and found to be 4.18 kN (0.94 kip) and 6.30 kN (1.42 kip), respectively.

Comparison of predicted and experimental deflection

Table 6 shows the experimental (Δ_{exp}) and the ACI-predicted post-crack deflection (Δ_{pre}), along with the comparison between them, at the different service-load thresholds. Because all of the slabs cracked above the calculated P_{serv} and the deflection of the uncracked sections was not of interest, the serviceability-limit values were set at 53% (P_n^c) and 67% (P_n^b) of the nominal strength, with ϕ and $C_e = 1$ (P_n^a). These service-load values, as well as the ACI-predicted load-deflection curve, are shown in Fig. 10. On average, the experimental to predicted deflections ($\Delta_{exp}/\Delta_{pre}$) for FC25 elements at P_n^c were between 0.94 and 1.12, and at P_n^b were between 0.87 and 0.96. For SW60 samples,

Table 4—Details of experimental and predicted nominal moment capacity

Group slab notation	Flexural test results		Analytical predictions	ACI 440-15 predictions			
	M_{exp}		$M_{n(an)}$	$M_{n(ACI)}$			
	kN·m (ft·kip)	CV %	kN·m (ft·kip)	kN·m (ft·kip)	$M_{exp}/M_{n(an)}$	$M_{exp}/M_{n(ACI)}$	M_{exp}/M_{des}
F-FC25-1	7.28 (5.37)	3.0	7.37 (5.43)	7.14 (5.27)	0.99	1.02	2.70
F-FC25-6	7.18 (5.29)	0.3	7.37 (5.43)	7.14 (5.26)	0.97	1.01	2.66
F-FC25-12	7.26 (5.36)	4.6	7.37 (5.44)	7.16 (5.28)	0.99	1.01	2.70
F-FC25-24	6.88 (5.07)	6.3	7.37 (5.44)	7.15 (5.28)	0.93	0.96	2.55
Average					0.97	1.0	2.65
F-SW60-1	6.88 (5.08)	12.1	7.36 (5.43)	7.12 (5.25)	0.93	0.97	2.55
F-SW60-6	6.48 (4.78)	1.9	7.36 (5.43)	7.13 (5.26)	0.88	0.91	2.40
F-SW60-12	6.38 (4.70)	6.4	7.37 (5.44)	7.15 (5.28)	0.87	0.89	2.37
F-SW60-24	6.03 (4.45)	1.3	7.36 (5.43)	7.13 (5.26)	0.82	0.84	2.24
Average					0.87	0.90	2.39
S-FC25-1	6.85 (5.05)	2.5	7.37 (5.44)	7.16 (5.28)	0.93	0.96	2.54
S-FC25-6	6.83 (5.04)	2.4	7.36 (5.43)	7.13 (5.26)	0.93	0.96	2.53
S-FC25-12	6.80 (5.01)	1.5	7.36 (5.43)	7.11 (5.24)	0.92	0.96	2.52
S-FC25-24	6.45 (4.76)	5.8	7.36 (5.43)	7.12 (5.25)	0.88	0.91	2.40
Average					0.91	0.94	2.50
S-SW60-1	6.20 (4.57)	11.3	7.37 (5.44)	7.16 (5.28)	0.84	0.87	2.30
S-SW60-6	6.00 (4.43)	13.1	7.36 (5.43)	7.14 (5.26)	0.81	0.84	2.23
S-SW60-12	5.27 (3.89)	5.6	7.36 (5.43)	7.12 (5.25)	0.72	0.74	1.96
S-SW60-24	5.46 (4.03)	6.1	7.36 (5.43)	7.11 (5.25)	0.74	0.77	2.03
Average					0.78	0.80	2.13

Note: M_{des} = 2.69 kN·m (1.99 ft·kip).

Table 5—First cracking load for all tested slabs

Group slab notation	Flexural test results		ACI 440-15 predictions	
	$P_{cr\ exp}$		$P_{cre\ pre}$	
	kN (kip)	COV %	kN (kip)	$P_{cr\ exp}/P_{cr\ pre}$
F-FC25-1	10.01 (2.25)	3.60	13.02 (2.93)	0.77
F-FC25-6	15.75 (3.54)	7.20	12.91 (2.90)	1.22
F-FC25-12	11.53 (2.59)	10.80	13.75 (3.09)	0.84
F-FC25-24	11.47 (2.58)	11.40	13.41 (3.01)	0.85
Average				0.92
F-SW60-1	9.88 (2.22)	11.60	12.50 (2.81)	0.79
F-SW60-6	11.54 (2.59)	11.20	12.62 (2.84)	0.91
F-SW60-12	13.19 (2.97)	9.60	13.35 (3.00)	0.99
F-SW60-24	15.31 (3.44)	14.00	12.84 (2.89)	1.19
Average				0.97
S-FC25-1	8.94 (2.01)	0.70	13.65 (3.07)	0.66
S-FC25-6	9.30 (2.09)	13.50	12.64 (2.84)	0.74
S-FC25-12	6.32 (1.42)	0.20	12.11 (2.72)	0.52
S-FC25-24	7.68 (1.73)	13.40	12.25 (2.75)	0.63
Average				0.63
S-SW60-1	11.88 (2.67)	15.90	13.49 (3.03)	0.88
S-SW60-6	10.22 (2.30)	2.45	12.84 (2.89)	0.80
S-SW60-12	9.12 (2.05)	10.80	12.40 (2.79)	0.74
S-SW60-24	8.37 (1.88)	6.50	12.16 (2.73)	0.69
Average	—			0.78

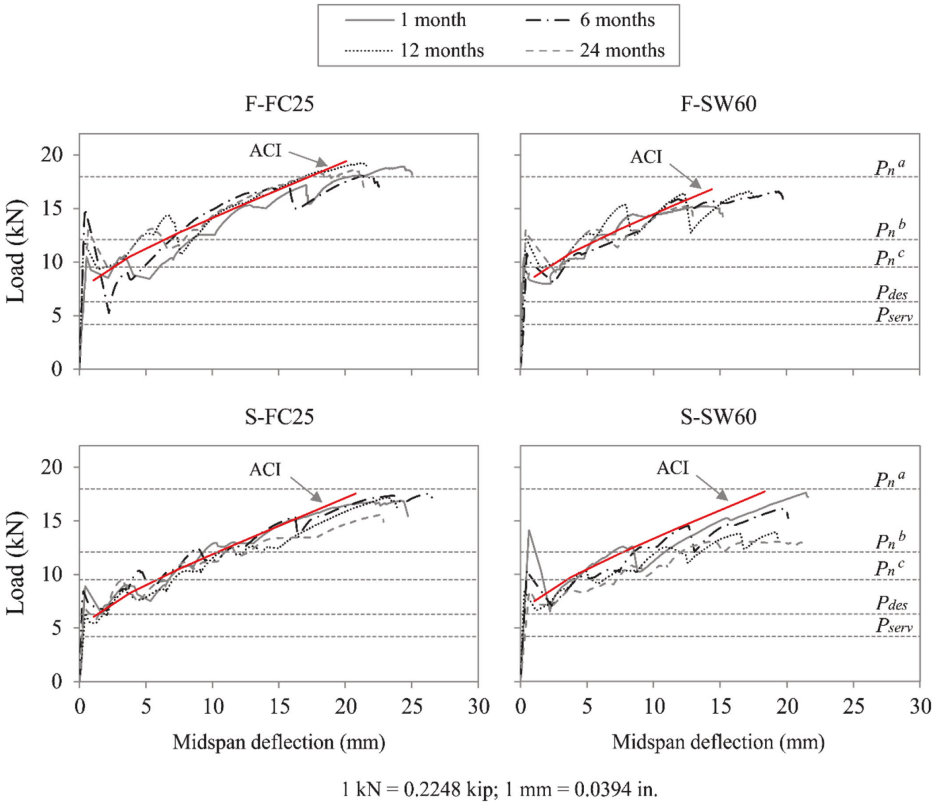

1 kN = 0.2248 kip; 1 mm = 0.0394 in.

Fig. 10—Experimental load-deflection curve of representative GFRP-RC slabs. Note: P_n^a *is nominal strength with* ϕ *and* C_e *= 1;* P_n^b *is nominal strength with* $\phi = 1$ *and* $C_e = 0.7$*; and* P_n^c *is nominal strength with* $C_e = 1$ *and* $\phi = 0.55$.

Table 6—Comparison of measured and predicted deflections

	Deflection at P_n^c			Deflection at P_n^b		
	Δ_{exp}	Δ_{pre}		Δ_{exp}	Δ_{pre}	
Group slab notation	mm (in.)	mm (in.)	$\Delta_{exp}/\Delta_{pre}$	mm (in.)	mm (in.)	$\Delta_{exp}/\Delta_{pre}$
F-FC25-1	2.00 (0.08)	2.54 (0.10)	0.79	6.79 (0.27)	6.35 (0.25)	1.07
F-FC25-6	3.81 (0.15)		1.50	5.46 (0.22)		0.86
F-FC25-12	2.48 (0.10)		0.98	4.57 (0.18)		0.72
F-FC25-24	3.13 (0.12)		1.23	5.21 (0.21)		0.82
Average			1.12			0.87
F-SW60-1	2.29 (0.09)	2.08 (0.08)	1.10	6.18 (0.24)	5.72 (0.23)	1.08
F-SW60-6	2.97 (0.12)		1.43	5.43 (0.21)		0.95
F-SW60-12	2.73 (0.11)		1.31	4.95 (0.20)		0.87
F-SW60-24	2.85 (0.11)		1.37	5.93 (0.23)		1.04
Average			1.30			0.98
S-FC25-1	5.99 (0.24)	5.66 (0.22)	1.06	9.80 (0.39)	10.41 (0.41)	0.94
S-FC25-6	3.86 0.15)		0.68	8.23 (0.32)		0.79
S-FC25-12	7.39 (0.29)		1.30	10.77 (0.42)		1.03
S-FC25-24	4.08 (0.16)		0.72	11.31 (0.45)		1.09
Average			0.94			0.96
S-SW60-1	3.71 (0.15)	3.56 (0.14)	1.04	8.02 (0.32)	7.75 (0.31)	1.03
S-SW60-6	3.43 (0.14)		0.96	7.59 (0.30)		0.98
S-SW60-12	5.25 (0.21)		1.48	11.15 (0.44)		1.44
S-SW60-24	7.99 (0.31)		2.25	13.22 (0.52)		1.71
Average			1.43			1.29

Note: P_n^c = 9.52 kN (2.14 kip); P_n^b = 12.10 kN (2.71 kip).

the average $\Delta_{exp}/\Delta_{pre}$ ratio at P_n^c ranged between 1.30 and 1.43, whereas at P_n^b it ranged between 0.98 to 1.29.

Overall, the measured midspan deflections at P_n^c and P_n^b are in acceptable agreement with the results obtained by the ACI 440.1R-15[8] guide, considering that the experimental-to-predicted ratio values are significantly sensitive to slight variations because of the relatively small measurements. Nonetheless, the largest deviations were noticed for accelerated-aged specimens.

Degradation mechanisms of GFRP bars

Based on the flexural test results, it can be interpreted that, because the slabs were designed to fail due to FRP bar rupture, some degradation occurred, affecting the ultimate tensile load capacity of the GFRP bars. Tensile strength reduction in FRP composites is largely due to a combination of different factors concerning fiber integrity and damage at the fiber/resin interface.[19,20] The former is associated with the resistance (at the fiber level) of the fiber itself against alkaline/chemical attack, while the latter is more related to the resin matrix softening and/or debonding at the interface. These degradation mechanisms affect the way the load is transferred between the fibers and the resin matrix, causing premature tensile failure. Durability mechanisms are interrelated and are known to be initiated by hydrolysis reaction and moisture absorption (diffusion through the resin matrix).[19,27]

Regardless of whether the concrete slabs were fully saturated or not, GFRP bars embedded in concrete can absorb moisture and water contained in the capillary pores, which seep into the resin matrix, thus affecting the fiber/resin interface.[23,64] It has been estimated that at 70% RH, the capillary and absorbed water in the concrete is approximately 21%.[65] The presence of absorbed moisture at high loads can induce local stress concentrations at the fiber/resin interface, which triggers cracks and debonding between the fiber and the resin matrix, leading to a reduction in the ultimate tensile strength.

It is evident that concrete elements subjected to seawater at 60°C (140°F) (SW60 specimens) were more affected by environmental conditioning compared to typical field exposure (13.8 to 17.5% difference). This emphasizes that the temperature and ambient RH have a considerable impact on the degradation of GFRP bars embedded in concrete. For this reason, GFRP-RC elements used in dry field applications would have better durability performance as opposed to fully saturated concrete.[65]

It should be noted that the accelerated-aging parameters used in this study (continuous, direct exposure of seawater at 60°C [140°F]) were very aggressive and highly unlikely, as the highest recorded punctual sea surface temperatures worldwide are approximately 35°C (95°F).[66] The correlation between accelerated conditioning and natural aging has not been established and is outside the scope of this

project. Additionally, current design provisions based on ACI 440.1R-15[8] remain conservative even for elements subjected to accelerated conditioning. The physico-mechanical test results on the durability of GFRP reinforcing bars embedded in seaconcrete related to this study can be found in Morales et al.[45]

SUMMARY AND CONCLUSIONS

A total of 48 glass fiber-reinforced polymer (GFRP)-reinforced concrete (RC) slabs strips with dimensions of 1828 mm (72 in.) long, 304 mm (12 in.) wide, and 152 mm (6 in.) depth reinforced with a 9.5 mm (0.375 in.) diameter GFRP bar were fabricated using two different seaconcrete mixture designs. All GFRP-RC slabs were exposed to accelerated aging and field conditioning over 24 months. Three-point flexural tests were performed on all the GFRP-RC slabs, over a clear span of 1524 mm (60 in.), after the specified exposure periods (1, 6, 12, or 24 months). The strength capacities were calculated using an analytical and simplified (ACI 440.1R-15[8]) approach. Test results were compared to the predicted values in terms of the flexural performance (first crack, ultimate and design capacity, and deflection). Based on the results, the main findings can be summarized as follows:

- The seaconcrete cylinders conditioned in seawater at 60°C (140°F) exhibited comparable compressive strength to samples exposed to field conditioning after 24 months of exposure, with a maximum average difference of 8.2% and 1.3% for Mixture Type-F and Type-S, respectively.
- After 24 months of exposure, the ultimate load capacity of the GFRP-RC slabs exposed to seawater at 60°C (140°F) was 13.8% and 17.5% lower than those conditioned in the field environment for Mixture Type-F and Type-S, respectively. However, the accelerated-aging parameters used are not yet correlated to real-life applications; thus, results must be calibrated with existing aged GFRP-RC structures.
- The analytical approach without any strength reduction factor (that is, using pristine bar properties) reasonably predicted the experimental failure moment capacity in most of the tested GFRP-RC slabs, specifically, for those exposed to field conditioning with an average $M_{exp}/M_{n(an)}$ of 0.97 (Type-F) and 0.91 (Type-S). In contrast, for those subjected to accelerated aging, it was 0.87 (Type-F) and 0.78 (Type-S), as expected, because ultimate capacity decreased.
- On average, the simplified conservative equations provided in ACI 440.1R-15[8] predicted a 3% lower failure moment capacity than analytically computed. The average $M_{exp}/M_{n(an)}$ for field conditioning resulted in 1.0 (Type-F) and 0.94 (Type-S), while for those exposed to accelerated aging was 0.90 (Type-F) and 0.80 (Type-S).
- The recorded ultimate moment capacity for all the GFRP-RC slabs was on average 2.13 to 2.65 times higher than the ACI 440.1R-15[8] predicted design load capacity. This is obviously attributed to the application of various knock-down factors (that is, C_E, ϕ, and f_{fu}^*) that make the design conservative even for elements subjected to accelerated conditioning.
- In general, all the simply supported one-way GFRP-RC slabs tested under the three-point bending behaved similarly and exhibited a bilinear trend, with a pre- and post-cracking response, regardless of the environmental conditioning or time of exposure.
- Overall, the ACI 440.1R-15[8] equations reasonably predicted the experimentally measured deflections based on a similar approximate onset cracking response. However, some deviations were observed, mainly for specimens conditioned in seawater at 60°C (140°F).

The findings of this study can be used to evaluate the long-term flexural performance of seaconcrete GFRP-RC slabs and the contribution of reduction factors to the design capacity. The authors recognize that the results presented in this study provided insight into mechanical performance solely on the specified type of concrete and GFRP reinforcing bar.

AUTHOR BIOS

ACI member **Carlos N. Morales** *is a PhD Candidate in the Department of Civil, Architectural, and Environmental Engineering at the University of Miami, Coral Gables, FL. He received his BS from the University of Puerto Rico at Mayagüez, Mayagüez, PR, and his MArch from the University of Miami. His research interests include the use of fiber-reinforced polymer (FRP) composites in reinforced concrete structures.*

ACI member **Guillermo Claure** *received his PhD from the University of Miami, where he served as a Lecturer and Senior Research Associate. He received his BS in civil engineering from Florida International University, Miami, FL. His research interests include the sustainability of structures, implementation of composite materials, and structural performance.*

Antonio Nanni, *FACI, is the Inaugural Senior Scholar, Professor, and Chair of the Department of Civil, Architectural, and Environmental Engineering at the University of Miami. He was the Founding Chair and is a member of ACI Committee 440, Fiber-Reinforced Polymer Reinforcement. His research interests include construction materials and their structural performance and field applications, including monitoring and renewal.*

ACKNOWLEDGMENTS

The authors gratefully acknowledge the financial support from the Qatar National Research Fund by Grant No. NPRP9-110-2-052, and the National Science Foundation (NSF) and its Industry-University Center for the Center for the Integration of Composites into Infrastructure (CICI) at the University of Miami under grant No. NSF-1916342. The contents stated herein are solely the responsibility of the authors.

REFERENCES

1. Hamilton, H. R.; Benmokrane, B.; Dolan, C. W.; and Sprinkel, M. M., "Polymer Materials to Enhance Performance of Concrete in Civil Infrastructure," *Polymer Reviews*, V. 49, No. 1, 2009, pp. 1-24. doi: 10.1080/15583720802656153

2. Bentur, A.; Berke, N.; and Diamond, S., *Steel Corrosion in Concrete: Fundamentals and Civil Engineering Practice*, CRC Press, London, UK, 1997, 208 pp.

3. Koch, G. H.; Brongers, M. P. H.; Thompson, N. G.; Virmani, Y. P.; and Payer, J. H., "Corrosion Cost and Preventive Strategies in the United States," FHWA-RD-01-156, Federal Highway Administration, McLean, VA, 2002, 786 pp.

4. Uddin, N., *Developments in Fiber-Reinforced Polymer (FRP) Composites for Civil Engineering*, first edition, Woodhead Publishing Limited, Sawston, UK, 2013, 525 pp.

5. Benmokrane, B.; Mohamed, H.; and Ahmed, E., "Recent Developments of FRP Bars as Internal Reinforcement in Concrete Structures & Field Applications," Fourth International Conference on Sustainable Construction Materials and Technologies, Las Vegas, NV, 2016, 10 pp.

6. Zoghi, M., *The International Handbook of FRP Composites in Civil Engineering*, CRC Press, Boca Raton, FL, 2013, 706 pp.

7. Emparanza, A. R.; Kampmann, R.; and De Caso y Basalo, F., "State-of-the-Practice of Global Manufacturing of FRP Rebar and Specifications," *The 13th International Symposium on Fiber-Reinforced Polymer Reinforcement for Concrete Structures*, SP-327, ACI Committee 440, R. El-Hacha, L. (D.) Cheng, M. Lopez de Murphy, and W. J. Gold, eds., American Concrete Institute, Farmington Hills, MI, 2017, pp 45.1-45.14.

8. ACI Committee 440, "Guide for the Design and Construction of Structural Concrete Reinforced with Fiber-Reinforced Polymer (FRP) Bars (ACI 440.1R-15)," American Concrete Institute, Farmington Hills, MI, 2015, 88 pp.

9. Xiao, J.; Qiang, C.; Nanni, A.; and Zhang, K., "Use of Sea-Sand and Seawater in Concrete Construction: Current Status and Future Opportunities," *Construction and Building Materials*, V. 155, Nov. 2017, pp. 1101-1111.

10. Younis, A.; Ebead, U.; Suraneni, P.; and Nanni, A., "Fresh and Hardened Properties of Seawater-Mixed Concrete," *Construction and Building Materials*, V. 190, Nov. 2018, pp. 276-286.

11. Khatibmasjedi, M.; Ramanathan, S.; Suraneni, P.; and Nanni, A., "Compressive Strength Development of Seawater-Mixed Concrete Subject to Different Curing Regimes," *ACI Materials Journal*, V. 117, No. 5, Sept. 2020, pp. 3-12. doi: 10.14359/51725973

12. El-Hassan, H., and El Maaddawy, T., "Microstructure Characteristics of GFRP Reinforcing Bars in Harsh Environment," *Advances in Materials Science and Engineering*, V. 2019, 2019, Article ID No. 8053843.

13. Chen, Y.; Davalos, J. F.; and Ray, I., "Durability Prediction for GFRP Reinforcing Bars Using Short-Term Data of Accelerated Aging Tests," *Journal of Composites for Construction*, ASCE, V. 10, No. 4, Aug. 2006, pp. 279-286. doi: 10.1061/(ASCE)1090-0268(2006)10:4(279)

14. Wang, Z.; Zhao, X.-L.; Xian, G.; Wu, G.; Singh Raman, R. K.; Al-Saadi, S.; and Haque, A. "Long-Term Durability of Basalt- and Glass-Fibre Reinforced Polymer (BFRP/GFRP) Bars in Seawater and Sea Sand Concrete Environment," *Construction and Building Materials*, V. 139, May 2017, pp. 467-489.

15. Al-Salloum, Y. A.; El-Gamal, S.; Almusallam, T. H.; Alsayed, S. H.; and Aqel, M., "Effect of Harsh Environmental Conditions on the Tensile Properties of GFRP Bars," *Composites Part B: Engineering*, V. 45, No. 1, Feb. 2013, pp. 835-844. doi: 10.1016/j.compositesb.2012.05.004

16. Wang, Z.; Zhao, X.-L.; Xian, G.; Wu, G.; Singh Raman, R. K.; and Al-Saadi, S., "Durability Study on Interlaminar Shear Behaviour of Basalt-, Glass- and Carbon-Fibre Reinforced Polymer (B/G/CFRP) Bars in Seawater Sea Sand Concrete Environment," *Construction and Building Materials*, V. 156, Dec. 2017, pp. 985-1004.

17. Tu, J.; Xie, H.; and Gao, K., "Prediction of the Long-Term Performance and Durability of GFRP Bars under the Combined Effect of a Sustained Load and Severe Environments," *Materials (Basel)*, V. 13, No. 10, May 2020, p. 2341. doi: 10.3390/ma13102341

18. Debaiky, A. S.; Nkurunziza, G.; Benmokrane, B.; and Cousin, P., "Residual Tensile Properties of GFRP Reinforcing Bars after Loading in Severe Environments," *Journal of Composites for Construction*, ASCE, V. 10, No. 5, Oct. 2006, pp. 370-380. doi: 10.1061/(ASCE)1090-0268(2006)10:5(370)

19. Chen, Y.; Davalos, J. F.; Ray, I.; and Kim, H.-Y., "Accelerated Aging Tests for Evaluations of Durability Performance of FRP Reinforcing Bars for Concrete Structures," *Composite Structures*, V. 78, No. 1, Mar. 2007, pp. 101-111. doi: 10.1016/j.compstruct.2005.08.015

20. Fergani, H.; Di Benedetti, M.; Miàs Oller, C.; Lynsdale, C.; and Guadagnini, M., "Durability and Degradation Mechanisms of GFRP Reinforcement Subjected to Severe Environments and Sustained Stress," *Construction and Building Materials*, V. 170, May 2018, pp. 637-648.

21. Almusallam, T. H.; Al-Salloum, Y. A.; Alsayed, S. H.; El-Gamal, S.; and Aqel, M., "Tensile Properties Degradation of Glass Fiber-Reinforced Polymer Bars Embedded in Concrete Under Severe Laboratory and Field Environmental Conditions," *Journal of Composite Materials*, V. 47, No. 4, 2013, pp. 393-407. doi: 10.1177/0021998312440473

22. Robert, M.; Cousin, P.; and Benmokrane, B., "Durability of GFRP Reinforcing Bars Embedded in Moist Concrete," *Journal of Composites for Construction*, ASCE, V. 13, No. 2, Apr. 2009, pp. 66-73. doi: 10.1061/(ASCE)1090-0268(2009)13:2(66)

23. Robert, M., and Benmokrane, B. "Combined Effects of Saline Solution and Moist Concrete on Long-Term Durability of GFRP Reinforcing Bars," *Construction and Building Materials*, V. 38, Jan. 2013, pp. 274-284.

24. Jia, D.; Guo, Q.; Mao, J.; Lv, J.; and Yang, Z., "Durability of Glass Fibre-Reinforced Polymer (GFRP) Bars Embedded in Concrete Under Various Environments. I: Experiments and Analysis," *Composite Structures*, V. 234, Feb. 2020, Article No. 111687. doi: 10.1016/j.compstruct.2019.111687

25. Trejo, D.; Gardoni, P.; and Kim, J. J., "Long-Term Performance of Glass Fiber-Reinforced Polymer Reinforcement Embedded in Concrete," *ACI Materials Journal*, V. 108, No. 6, Nov.-Dec. 2011, pp. 605-613.

26. Khatibmasjedi, M.; Ramanathan, S.; Suraneni, P.; and Nanni, A., "Durability of Commercially Available GFRP Reinforcement in Seawater-Mixed Concrete under Accelerated Aging Conditions," *Journal of Composites for Construction*, ASCE, V. 24, No. 4, 2020, p. 04020026. doi: 10.1061/(ASCE)CC.1943-5614.0001035

27. El-Hassan, H.; El-Maaddawy, T.; Al-Sallamin, A.; and Al-Saidy, A., "Performance Evaluation and Microstructural Characterization of GFRP Bars in Seawater-Contaminated Concrete," *Construction and Building Materials*, V. 147, Aug. 2017, pp. 66-78.

28. El-Salakawy, E., and Benmokrane, B., "Serviceability of Concrete Bridge Deck Slabs Reinforced with Fiber-Reinforced Polymer Composite Bars," *ACI Structural Journal*, V. 101, No. 5, Sept.-Oct. 2004, pp. 727-736.

29. Ali, A. H.; Afifi, M. Z.; Abdulsalam, B.; Haggag, H.; El Hashimy, A.; El-Sayed, T.; and Mohamed, H. M., "Performance Evaluation of One-Way Concrete Slabs Reinforced with New Developed GFRP Bars," *Materials Sciences and Applications*, V. 6, No. 5, 2015, pp. 420-435. doi: 10.4236/msa.2015.65046

30. Kara, I. F.; Köroğlu, M. A.; and Ashour, A. F., "Tests of Continuous Concrete Slabs Reinforced with Basalt Fiber-Reinforced Plastic Bars," *ACI Structural Journal*, V. 114, No. 5, Sept.-Oct. 2017, pp. 1201-1213. doi: 10.14359/51689784

31. Mahroug, M. E. M.; Ashour, A. F.; and Lam, D., "Tests of Continuous Concrete Slabs Reinforced with Carbon Fibre Reinforced Polymer Bars," *Composites Part B: Engineering*, V. 66, Nov. 2014, pp. 348-357.

32. Lotfy, E. M.; Elzeiny, S. M.; and Rashad, A. M., "Flexural Capacity of One-Way GFRP Concrete Slabs," *Proceedings of the Institution of Civil Engineers - Construction Materials*, V. 164, No. 3, June 2011, pp. 143-152.

33. Michaluk, C. R.; Rizkalla, S. H.; Tadros, G.; and Benmokrane, B., "Flexural Behavior of One-Way Concrete Slabs Reinforced by Fiber Reinforced Plastic Reinforcements," *ACI Structural Journal*, V. 95, No. 3, May-June 1998, pp. 353-364.

34. Attia, K.; El Refai, A.; and Alnahhal, W., "Flexural Behavior of Basalt Fiber–Reinforced Concrete Slab Strips with BFRP Bars: Experimental Testing and Numerical Simulation," *Journal of Composites for Construction*, ASCE, V. 24, No. 2, Apr. 2020, p. 04020007. doi: 10.1061/(ASCE)CC.1943-5614.0001002

35. Bowen, G.; Zheng, P.; Moen, C. D.; and Sharp, S. R., "Flexural Behavior at Service and Ultimate Limit State of One-Way Concrete Slabs Reinforced with Corrosion-Resistant Reinforcing Bars," *Transportation Research Record: Journal of the Transportation Research Board*, V. 2331, No. 1, 2013, pp. 47-58. doi: 10.3141/2331-05

36. Nanni, A., "Flexural Behavior and Design of RC Members Using FRP Reinforcement," *Journal of Structural Engineering*, ASCE, V. 119, No. 11, Nov. 1993, pp. 3344-3359. doi: 10.1061/(ASCE)0733-9445(1993)119:11(3344)

37. Ombres, L.; Alkhrdaji, T.; and Nanni, A., "Flexural Analysis of One-Way Concrete Slabs Reinforced with GFRP Rebars," I. Crivelli-Visconti, ed., *International Meeting on Composite Materials, PLAST 2000, Proceedings, Advancing with Composites 2000*, Milan, Italy, 2000, pp. 243-250.

38. Al-Sunna, R.; Pilakoutas, K.; Hajirasouliha, I.; and Guadagnini, M., "Deflection Behaviour of FRP Reinforced Concrete Beams and Slabs: An Experimental Investigation," *Composites Part B: Engineering*, V. 43, No. 5, July 2012, pp. 2125-2134. doi: 10.1016/j.compositesb.2012.03.007

39. Chang, K., and Seo, D., "Behavior of One-Way Concrete Slabs Reinforced with GFRP Bars," *Journal of Asian Architecture and Building Engineering*, V. 11, No. 2, 2012, pp. 351-358. doi: 10.3130/jaabe.11.351

40. Gao, Y.; Zhou, Y.; Zhou, J.; Kong, X.; Zhang, B.; Liu, S.; Feng, J.; Zhu, N.; Fan, H.; and Jin, F., "Blast Responses of One-Way Sea-Sand Seawater Concrete Slabs Reinforced with BFRP Bars," *Construction and Building Materials*, V. 232, Jan. 2020, Article No. 117254.

41. Dong, Z.; Wu, G.; Zhao, X.-L.; Zhu, H.; and Lian, J.-L., "Durability Test on the Flexural Performance of Seawater Sea-Sand Concrete Beams Completely Reinforced with FRP Bars," *Construction and Building Materials*, V. 192, Dec. 2018, pp. 671-682.

42. Younis, A.; Ebead, U.; Suraneni, P.; and Nanni, A., "Short-Term Flexural Performance of Seawater-Mixed Recycled-Aggregate GFRP-Reinforced Concrete Beams," *Composite Structures*, V. 236, Mar. 2020, Article No. 111860. doi: 10.1016/j.compstruct.2020.111860

43. Turner, J. R., and Thayer, J. F., *Introduction to Analysis of Variance: Design, Analysis & Interpretation*, SAGE Publications, Inc., Thousand Oaks, CA, 2001, 192 pp.

44. SEACON, "Sustainable Concrete Using Seawater, Salt-Contaminated Aggregates, and Non-Corrosive Reinforcement," *Deliverable D2.4*, 2015, 44 pp.

45. Morales, C. N.; Claure, G.; Emparanza, A. R.; and Nanni, A., "Durability of GFRP Reinforcing Bars in Seawater Concrete," *Construction and Building Materials*, V. 270, Feb. 2021, Article No. 121492.

46. Otsuki, N.; Min,, A. K.; ; and Nagata,, T.; , and Yi,, C., "Durability of Seawater Mixed Concrete with Different Replacement Ratio of BFS

(Blast Furnace Slag) and FA (Fly Ash)," *Journal of Civil Engineering and Architecture*, V. 10, No. 5, 2016, pp. 568-580.

47. Younis, A.; Ebead, U.; Suraneni, P.; and Nanni, A., "Performance of Seawater-Mixed Recycled-Aggregate Concrete," *Journal of Materials in Civil Engineering*, ASCE, V. 32, No. 1, Jan. 2020, p. 04019331. doi: 10.1061/(ASCE)MT.1943-5533.0002999

48. Montanari, L.; Suraneni, P.; Tsui-Chang, M.; Khatibmasjedi, M.; Ebead, U.; Weiss, J.; and Nanni, A., "Hydration, Pore Solution, and Porosity of Cementitious Pastes Made with Seawater," *Journal of Materials in Civil Engineering*, ASCE, V. 31, No. 8, Aug. 2019, p. 04019154. doi: 10.1061/(ASCE)MT.1943-5533.0002818

49. ASTM C39/C39M-17, "Standard Test Method for Compressive Strength of Cylindrical Concrete Specimens," ASTM International, West Conshohocken, PA, 2017, 8 pp.

50. ASTM D2584-18, "Standard Test Method for Ignition Loss of Cured Reinforced Resins," ASTM International, West Conshohocken, PA, 2018, 3 pp.

51. ASTM D7957/D7957M-17, "Standard Specification for Solid Round Glass Fiber Reinforced Polymer Bars for Concrete Reinforcement," ASTM International, West Conshohocken, PA, 2017, 5 pp.

52. ASTM D7205/D7205M-16, "Standard Test Method for Tensile Properties of Fiber Reinforced Polymer Matrix Composite Bars," ASTM International, West Conshohocken, PA, 2016, 13 pp.

53. Morales, C. N.; Claure, G.; Álvarez, J.; and Nanni, A., "Evaluation of Fiber Content in GFRP Bars Using Digital Image Processing," *Composites Part B: Engineering*, V. 200, Nov. 2020, Article No. 108307.

54. ACI Committee 437, "Code Requirements for Load Testing of Existing Concrete Structures (ACI 437-12) and Commentary (ACI 437R-12)," American Concrete Institute, Farmington Hills, MI, 2012.

55. Bank, L. C., *Composites for Construction: Structural Design with FRP Materials*, John Wiley & Sons, Inc., Hoboken, NJ, 2006, 560 pp.

56. Nanni, A.; De Luca, A.; and Jawaheri Zadeh, H., *Reinforced Concrete with FRP Bars: Mechanics and Design*, CRC Press/Taylor & Francis Group, Boca Raton, FL, 2014, 418 pp.

57. Todeschini, C. E.; Bianchini, A. C.; and Kesler, C. E., "Behavior of Concrete Columns Reinforced with High Strength Steels," *ACI Journal Proceedings*, V. 61, No. 6, June 1964, pp. 701-716.

58. Balaguru, P.; Nanni, A.; and Giancaspro, J., *FRP Composites for Reinforced and Prestressed Concrete Structures*, CRC Press/Taylor & Francis Group, New York, NY, and London, UK, 2009, 336 pp.

59. Xue, W.; Peng, F.; and Zheng, Q., "Design Equations for Flexural Capacity of Concrete Beams Reinforced with Glass Fiber-Reinforced Polymer Bars," *Journal of Composites for Construction*, ASCE, V. 20, No. 3, June 2016, p. 04015069. doi: 10.1061/(ASCE)CC.1943-5614.0000630

60. ACI Committee 318, "Building Code Requirements for Structural Concrete (ACI 318-19) and Commentary (ACI 318R-19)," American Concrete Institute, Farmington Hills, MI, 2019, 624 pp.

61. Bischoff, P. H., and Gross, S. P., "Equivalent Moment of Inertia Based on Integration of Curvature," *Journal of Composites for Construction*, ASCE, V. 15, No. 3, June 2011, pp. 263-273. doi: 10.1061/(ASCE)CC.1943-5614.0000164

62. Mohammed, T. U.; Hamada, H.; and Yamaji, T., "Long-Term Durability of Concrete Made with Slag Cements under Marine Environment," *ACI Materials Journal*, V. 116, No. 5, Sept. 2019, pp. 5-16. doi: 10.14359/51716995

63. Vafaei, D.; Hassanli, R.; Ma, X.; Duan, J.; and Zhuge, Y., "Sorptivity and Mechanical Properties of Fiber-Reinforced Concrete Made with Seawater and Dredged Sea-Sand," *Construction and Building Materials*, V. 270, Feb. 2021, Article No 121436.

64. Manalo, A.; Maranan, G.; Benmokrane, B.; Cousin, P.; Alajarmeh, O.; Ferdous, W.; Liang, R.; and Hota, G., "Comparative Durability of GFRP Composite Reinforcing Bars in Concrete and in Simulated Concrete Environments," *Cement and Concrete Composites*, V. 109, May 2020, Article No. 103564. doi: 10.1016/j.cemconcomp.2020.103564

65. Huang, J., and Aboutaha, R., "Environmental Reduction Factors for GFRP Bars Used as Concrete Reinforcement: New Scientific Approach," *Journal of Composites for Construction*, ASCE, V. 14, No. 5, Oct. 2010, pp. 479-486. doi: 10.1061/(ASCE)CC.1943-5614.0000122

66. "Ocean: Sea Surface Temperature (1 Month - AVHRR, 1981-2006)," NASA Earth Observations.